A robust and well-balanced numerical model for solving the two-layer shallow water equations over uneven topography

CrossMark

Xinhua Lu [a],[*], Bingjiang Dong [b], Bing Mao [c], Xiaofeng Zhang [a]

[a] *State Key Laboratory of Water Resources and Hydropower Engineering Science, Wuhan University, Wuhan 430072, China*
[b] *Hydrology Bureau, Yangtze River Water Resource Commission, Wuhan 430010, China*
[c] *Yangtze River Scientific Research Institute, Wuhan 430015, China*

A R T I C L E   I N F O

A B S T R A C T

A robust and well-balanced numerical model is developed for solving the two-layer shallow water equations based on the approximate Riemann solver in the framework of finite-volume methods. The HLL (Harten, Lax, and van Leer) solver is employed to calculate the numerical fluxes. The numerical balance between the flux gradient and the source terms is achieved by using a balance-reformulation method. To obtain exactly the lake-at-rest solutions as the water depth is chosen as the conserved variable for the continuity equations, a modified HLL flux formulation is proposed for mass flux calculations. Several numerical tests used to validate the performance of the developed numerical model. The results show that the developed model is accurate, well balanced, and that it predicts no oscillations around large gradients.

© 2015 Académie des sciences. Published by Elsevier Masson SAS. All rights reserved.

1. Introduction

In this study, we consider a system with two superposed shallow flow layers. The fluids are assumed to be immiscible and of different but constant densities. Mathematically resolving of the two-layer shallow water equations (abbreviated as 2LSWE hereafter) is useful and of great importance for studying stratified flow motions, e.g., wave–mud interactions [1,2], thermally or salinity-driven exchange flow motions [3], internal wave behaviors in the continental shelf [4], and chaotic mixing of particles in layered flows [5].

Existing numerical schemes for solving the 2LSWE rely on the numerical techniques for solving the one-layer shallow water equation (1LSWE hereafter). In solving the 1LSWE, various tough issues were encountered, e.g., numerical oscillation or instability around shocks or discontinuities, generation of spurious flow over uneven topography caused by the numerical imbalance between the flux gradient and the source terms. The numerical techniques for resolving these difficulties related to the 1LSWE have been significantly advanced in recent years [6–8]. Compared with the situation in solving the 1LSWE, solving the 2LSWE is more complicated, since the coupling between the layers in the 2LSWE leads to a non-conservative product term. Moreover, it is non-trivial to devise well-balanced numerical schemes for the 2LSWE.

The non-conservative product term in the 2LSWE accounts for the momentum exchange between the layers. This term involves partial derivatives of the unknown physical variables that has no definition around shocks or discontinuities. Rigor-

---

* Corresponding author.

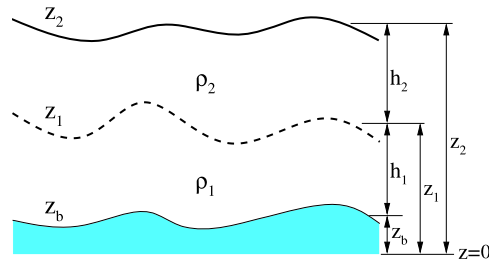*E-mail address:* xhluhh@whu.edu.cn (X. Lu).

Fig. 1. (Color online.) Definition sketch of a two-layer shallow water system.

ous theory for mathematically resolving the system with non-conservative terms has not been perfected yet. By choosing a specially designed coordinate system, Kurganov and Petrova [9] rewrote the 2LSWE system to make the effect of the nonconservative product term as small as possible. This scheme was verified to be robust when the fluctuation in the upper-layer surface is small. Dumbser et al. [10], and Castro-Díaz et al. [11] developed path-conservative numerical schemes for solving the 2LSWE based on the idea that the non-conservative product term can be interpreted as a Borel measure [12]. As pointed out by Abgrall and Karni [13], the path-conservative schemes may fail in obtaining reasonable solutions; for instance, may capture shocks incorrectly. Spinewine et al. [14] proposed an approach to make the non-conservative product term vanish by rearranging the governing equations.

The well-balanced property (e.g., the C-Property) is another objective to be achieved in developing numerical schemes for solving the 2LSWE involving source terms. The concept of the well-balanced property is originally proposed for solving the 1LSWE; it says that a numerical scheme should achieve a balance between the flux gradient and the source terms under steady stationary flow conditions [15]. A violation of this balance could trigger spurious flows and predict incorrect wave propagation speeds [16,17]. Various methods are proposed in the literature to tackle this imbalance problem in solving the 1LSWE. Several methods are verified to be robust and effective for solving the 1LSWE, e.g., the surface-gradient method [18], the hydraulic-reconstruction approach [19], and the surface-gradient-splitting approach [20,21]. However, when directly applying these approaches to solve the 2LSWE, some are found to be ineffective. For instance, as reported by Lee et al. [22,23], the surface-gradient splitting with a hydraulic reconstruction approach proposed by Liang and Borthwick [21], which exhibits the exactly well-balanced property for solving the 1LSWE, induces high spurious oscillations in the vicinity of discontinuities when used for solving the 2LSWE. The primary reason for explaining the different performances of a same method in solving the two different equation systems, lies in the existence of the non-conservative product term in the 2LSWE. As stated previously, this term is also a tough issue to be addressed.

The aim of this paper is to develop a robust and well-balanced numerical model for solving the 2LSWE with well treatment of the non-conservative product term. Special attention will be made to construct an effective numerical scheme to achieve exact lake-at-rest solutions for solving the 2LSWE.

The rest of the paper is organized as follows. Section 2 presents the numerical method for solving the 2LSWE. The general essentials and techniques for the numerical discretizations are presented. The method to achieve the well-balanced property is detailed. In Section 3, several numerical tests are presented to verify the performances of the numerical model. Finally, conclusions and discussions are given in Section 4.

2. Governing equations and numerical methods

In this paper, attention is focused on 1D flow in a channel with rectangular and constant-width cross sections. In principle, the numerical model developed below can be straightforwardly extended to 2D natural channels with complex geometry. The definition sketch for the 1D two-layer shallow water system is illustrated in Fig. 1. By neglecting the vertical acceleration effect and adopting the hydrostatic assumption, the 1D 2LSWE can be derived from the vertical 2D Reynolds-averaged Navier–Stokes equations. The governing equations for the upper layer are

$$\frac{\partial h_2}{\partial t} + \frac{\partial q_{x2}}{\partial x} = 0 \tag{1}$$

$$\frac{\partial q_{x2}}{\partial t} + \frac{\partial \left(u_2 q_{x2} + \frac{1}{2} g h_2^2 \right)}{\partial x} = -g h_2 \frac{\partial z_1}{\partial x} + \frac{\tau_{sx} - \tau_{wx}}{\rho_2} \tag{2}$$

and, for the lower layer,

$$\frac{\partial h_1}{\partial t} + \frac{\partial q_{x1}}{\partial x} = 0 \tag{3}$$

$$\frac{\partial q_{x1}}{\partial t} + \frac{\partial \left(u_1 q_{x1} + \frac{1}{2} g h_1^2 \right)}{\partial x} = -g h_1 \frac{\partial z_b}{\partial x} + \frac{\tau_{wx} - \tau_{bx}}{\rho_1} - \chi g h_1 \frac{\partial h_2}{\partial x} \tag{4}$$

Here, t denotes time; x is the streamwise coordinate; h_k is the layer depth with subscripts $k = 1$ and $k = 2$ representing the values corresponding to the lower and upper layers, respectively; q_{xk} is the discharge per unit width; $u_k = q_{xk}/h_k$ denotes the depth-averaged velocity of layer k; z_b is the bed elevation above a reference level; z_1 and z_2 denote the interface and upper-layer surface elevations with respect to the reference level and have the relation $z_1 = z_b + h_1$ and $z_2 = z_1 + h_2$; ρ_k is the flow density and $\chi = \rho_2/\rho_1$ is the density ratio between the layers; τ_{sx} is the external shear stress (e.g., wind stress) at the upper-layer surface; τ_{wx} denotes the shear stress at the interface between the layers and τ_{bx} is the bed friction force.

The governing equations for the upper layer (Eqs. (1)–(2)) are equivalent to the classic 1LSWE if the interface does not change with time. In this sense, the upper-layer equation system can be solved using existing effective 1LSWE solvers if the immobile interface profile is known a priori before the simulation. The governing equations for the lower layer (Eqs. (3)–(4)) is equivalent to the 1LSWE if and only if the non-conservative term $\chi g h_1 \frac{\partial h_2}{\partial x}$ vanishes (e.g., when $\chi = 0$ or $h_2 = \mathrm{constant}$).

To simplify the descriptions below, Eqs. (1)–(4) are recast into a vector form as

$$\frac{\partial \boldsymbol{U_k}}{\partial t} + \frac{\partial \boldsymbol{F_k}}{\partial x} = \boldsymbol{S_k} \tag{5}$$

where,

$$\boldsymbol{U_2} = \begin{bmatrix} h_2 \\ q_{x2} \end{bmatrix}, \; \boldsymbol{F_2} = \begin{bmatrix} q_{x2} \\ u_2 q_{x2} + \frac{1}{2} g h_2^2 \end{bmatrix}, \; \boldsymbol{S_2} = \begin{bmatrix} 0 \\ -g h_2 \dfrac{\partial z_1}{\partial x} \end{bmatrix} \tag{6}$$

and

$$\boldsymbol{U_1} = \begin{bmatrix} h_1 \\ q_{x1} \end{bmatrix}, \; \boldsymbol{F_1} = \begin{bmatrix} q_{x1} \\ u_1 q_{x1} + \frac{1}{2} g h_1^2 \end{bmatrix}, \; \boldsymbol{S_1} = \begin{bmatrix} 0 \\ -g h_1 \dfrac{\partial z_b}{\partial x} - \chi g h_1 \dfrac{\partial h_2}{\partial x} \end{bmatrix} \tag{7}$$

Note that the shear stresses at the upper-layer surface, interface, and at the lower-layer bottom are omitted to simplify the problem as was done in other literature reports [9,24,25]. The simplification here is also due to the fact that these terms generally cause no numerical inconveniences and the numerical methods developed below can be extended to incorporate these terms straightforwardly without any difficulty. For incorporating these shear stresses for simulations under practical situations, we refer to [1].

2.1. Processing the non-conservative product term

To treat the non-conservative product term in the 2LSWE, we follow the idea in [14,26] via rearranging the 2LSWE to make this term vanish. In observing that

$$-g h_1 \frac{\partial h_2}{\partial x} - g h_2 \frac{\partial z_1}{\partial x} \equiv -g h_1 \frac{\partial h_2}{\partial x} - g h_2 \left(\frac{\partial h_1}{\partial x} + \frac{\partial z_b}{\partial x} \right) \equiv -g \frac{\partial h_1 h_2}{\partial x} - g h_2 \frac{\partial z_b}{\partial x} \tag{8}$$

a combination of Eqs. (2) and (4) gives the following conservative momentum equation

$$\frac{\partial}{\partial t} \left(q_{x2} + \frac{1}{\chi} q_{x1} \right) + \frac{\partial}{\partial x} \left(u_2 q_{x2} + \frac{1}{\chi} u_1 q_{x1} + g h_1 h_2 + \frac{1}{2} g h_2^2 + \frac{1}{\chi} \frac{1}{2} g h_1^2 \right)$$

$$= -g h_2 \frac{\partial z_b}{\partial x} - \frac{1}{\chi} g h_1 \frac{\partial z_b}{\partial x} \tag{9}$$

A similar manipulation to Eqs. (1) and (3) gives the following combined continuity equation

$$\frac{\partial}{\partial t} \left(h_2 + \frac{1}{\chi} h_1 \right) + \frac{\partial}{\partial x} \left(q_{x2} + \frac{1}{\chi} q_{x1} \right) = 0 \tag{10}$$

In a vector form, the governing equations for the combined system can be written as

$$\frac{\partial \boldsymbol{U_w}}{\partial t} + \frac{\partial \boldsymbol{F_w}}{\partial x} = \boldsymbol{S_w} \tag{11}$$

where

$$\boldsymbol{U_w} = \begin{bmatrix} h_w \\ q_{xw} \end{bmatrix} = \begin{bmatrix} h_2 + \dfrac{1}{\chi} h_1 \\ q_{x2} + \dfrac{1}{\chi} q_{x1} \end{bmatrix}, \; \boldsymbol{S_w} = \begin{bmatrix} 0 \\ -g h_2 \dfrac{\partial z_b}{\partial x} - \dfrac{1}{\chi} g h_1 \dfrac{\partial z_b}{\partial x} \end{bmatrix}$$

$$\boldsymbol{F_w} = \begin{bmatrix} q_{x2} + \dfrac{1}{\chi} q_{x1} \\ u_2 q_{x2} + \dfrac{1}{\chi} u_1 q_{x1} + g h_1 h_2 + \dfrac{1}{2} g h_2^2 + \dfrac{1}{\chi} \dfrac{1}{2} g h_1^2 \end{bmatrix} \tag{12}$$

Here, the subscript 'w' denotes the term related to the combined system. Note that $h_w = h_2 + h_1/\chi$ is used as the equivalent depth for the combined system and for convenience, we define $H = h_1 + h_2$ as the locally total depth. In the rest of the paper, attention is focused on solving the 2LSWE based on Eqs. (5) and (11) with components for the upper layer and the combined system defined by Eqs. (6) and (12), respectively.

2.2. Well-balanced techniques

In this section, we devise a well-balanced numerical scheme for solving the 2LSWE. To achieve this, we firstly briefly describe the imbalance problem encountered in solving the 1LSWE, and also present a simple technique that will be used in solving the 2LSWE to overcome this problem.

2.2.1. One-layer imbalance problem and the balance-reformulation method

The governing equations related to the 1LSWE are the Saint-Venant equations, which in a compact and conservative vector form are expressed as

$$\frac{\partial \boldsymbol{U}}{\partial t} + \frac{\partial \boldsymbol{F}}{\partial x} = \boldsymbol{S} \tag{13}$$

where,

$$\boldsymbol{U} = \begin{bmatrix} U_c \\ U_m \end{bmatrix} = \begin{bmatrix} h \\ q_x \end{bmatrix}, \quad \boldsymbol{F} = \begin{bmatrix} F_c \\ F_m \end{bmatrix} = \begin{bmatrix} q_x \\ uq_x + \frac{1}{2}gh^2 \end{bmatrix}, \quad \boldsymbol{S} = \begin{bmatrix} S_c \\ S_m \end{bmatrix} = \begin{bmatrix} 0 \\ -gh\dfrac{\partial z_b}{\partial x} \end{bmatrix} \tag{14}$$

Here, the subscripts 'c' and 'm' denote the components related to the continuity and momentum equations, respectively. Symbols q_x, u, h, and z stand for the discharge per unit width, the velocity, the water depth, and the water surface elevation for the one-layer shallow-water system.

An explicit conservative finite volume discretization of Eq. (13) at cell i gives [21,27]

$$\boldsymbol{U}_i^{n+1} = \boldsymbol{U}_i^n - \frac{\Delta t}{\Delta x}\left(\boldsymbol{F}_{i+1/2} - \boldsymbol{F}_{i-1/2}\right) + \Delta t\, \boldsymbol{S}_i \tag{15}$$

Here we take the HLL (Harten, Lax, and van Leer) approximate Riemann solver [28], which is used in this paper, as an example to demonstrate the imbalance problem related to the discretization of the momentum equation. The HLL-formula-based numerical flux (abbreviated as HLL flux hereafter) is expressed as [28]

$$\boldsymbol{F}_{i-1/2}^{\text{HLL}} = \begin{bmatrix} F_{i-1/2}^{\text{HLL}_c} \\ F_{i-1/2}^{\text{HLL}_m} \end{bmatrix} \tag{16}$$

where

$$F_{i-1/2}^{\text{HLL}_c} = \frac{S_{i-1/2}^R F_{c,i-1/2}^L - S_{i-1/2}^L F_{c,i-1/2}^R}{S_{i-1/2}^R - S_{i-1/2}^L} + \frac{S_{i-1/2}^L S_{i-1/2}^R}{S_{i-1/2}^R - S_{i-1/2}^L}\left(h_{i-1/2}^R - h_{i-1/2}^L\right) \tag{17}$$

$$F_{i-1/2}^{\text{HLL}_m} = \frac{S_{i-1/2}^R F_{m,i-1/2}^L - S_{i-1/2}^L F_{m,i-1/2}^R}{S_{i-1/2}^R - S_{i-1/2}^L} + \frac{S_{i-1/2}^L S_{i-1/2}^R}{S_{i-1/2}^R - S_{i-1/2}^L}\left(q_{x,i-1/2}^R - q_{x,i-1/2}^L\right) \tag{18}$$

Here, $F_{i-1/2}^{\text{HLL}_c}$ and $F_{i-1/2}^{\text{HLL}_m}$ respectively denote the numerical flux for the continuity and momentum equations at the cell interface $i - 1/2$. The superscripts 'L' and 'R' denote the values corresponding to the left and right Riemann states at the cell interface. The S^L and S^R are the lower and upper bounds of wave speeds that are related to the local Riemann states of the velocity and water depth [6,29]. S^L and S^R can be estimated as, for the 1LSWE system [30],

$$S_{i-1/2}^L = \min\left(u_{i-1} - \sqrt{gh_{i-1}}, u_i - \sqrt{gh_i}\right)$$
$$S_{i-1/2}^R = \max\left(u_{i-1} + \sqrt{gh_{i-1}}, u_i + \sqrt{gh_i}\right) \tag{19}$$

and for the 2LSWE system [14]

$$S_{i-1/2}^L = \min\left(S_{1,i-1}^L, S_{1,i}^L, S_{2,i-1}^L, S_{2,i}^L, 0\right)$$
$$S_{i-1/2}^R = \max\left(S_{1,i-1}^R, S_{1,i}^R, S_{2,i-1}^R, S_{2,i}^R, 0\right) \tag{20}$$

where
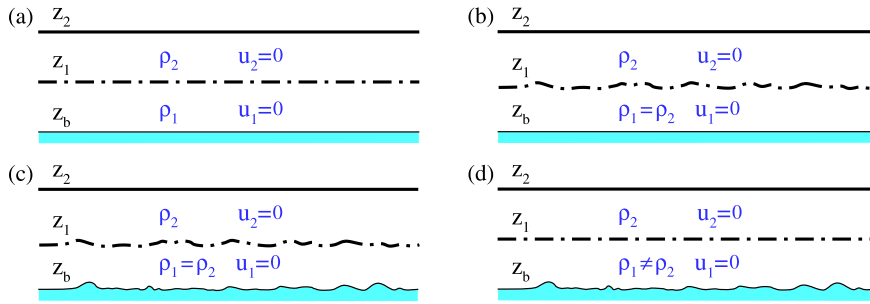
Fig. 2. (Color online.) Lake-at-rest configurations for the two-layer shallow-water system. The upper-layer surface and interface profiles are shown by the thick solid lines (——) and the dash-dotted lines (– · – · –), respectively. The shaded area covered with a thin solid line represents the bed topography.

$$S_{2,i}^{L} = u_{2,i} - \sqrt{gh_{2,i}}, \quad S_{1,i}^{L} = u_{1,i} - \sqrt{g(h_{1,i} + \chi h_{2,i})}$$
$$S_{2,i}^{R} = u_{2,i} + \sqrt{gh_{2,i}}, \quad S_{1,i}^{R} = u_{1,i} + \sqrt{g(h_{1,i} + \chi h_{2,i})} \tag{21}$$

By using a spatially first-order scheme and under a steady stationary flow condition, Eq. (18) reduces to

$$F_{i-1/2}^{\mathrm{HLL}m} = \frac{S_{i-1/2}^{R} \cdot \frac{1}{2}gh_{i-1}^{2} - S_{i-1/2}^{L} \cdot \frac{1}{2}gh_{i}^{2}}{S_{i-1/2}^{R} - S_{i-1/2}^{L}} \tag{22}$$

Similarly, we obtain the momentum flux at the cell interface $i + 1/2$ under a quiescent flow condition as

$$F_{i+1/2}^{\mathrm{HLL}m} = \frac{S_{i+1/2}^{R} \cdot \frac{1}{2}gh_{i}^{2} - S_{i+1/2}^{L} \cdot \frac{1}{2}gh_{i+1}^{2}}{S_{i+1/2}^{R} - S_{i+1/2}^{L}} \tag{23}$$

Then the flux gradient term in Eq. (15) for cell i, $\frac{1}{\Delta x}\left(F_{i+1/2}^{\mathrm{HLL}m} - F_{i-1/2}^{\mathrm{HLL}m}\right)$ can be calculated as

$$\frac{F_{i+1/2}^{\mathrm{HLL}m} - F_{i-1/2}^{\mathrm{HLL}m}}{\Delta x} = \frac{1}{\Delta x}\left[\frac{S_{i+1/2}^{R} \cdot \frac{1}{2}gh_{i}^{2} - S_{i+1/2}^{L} \cdot \frac{1}{2}gh_{i+1}^{2}}{S_{i+1/2}^{R} - S_{i+1/2}^{L}} - \frac{S_{i-1/2}^{R} \cdot \frac{1}{2}gh_{i-1}^{2} - S_{i-1/2}^{L} \cdot \frac{1}{2}gh_{i}^{2}}{S_{i-1/2}^{R} - S_{i-1/2}^{L}}\right] \tag{24}$$

As seen from Eq. (24), under a steady stationary flow condition, the discretized flux gradient term is so complex that generally it is non-trivial to discretize the bed-slope source term, $S_m = -gh\frac{\partial z_b}{\partial x}$ in Eq. (15), to exactly balance the flux gradient term shown in Eq. (24).

Note that the following relation exists

$$-\frac{\partial}{\partial x}\left(\frac{1}{2}gh^{2}\right) - gh\frac{\partial z_b}{\partial x} \equiv -gh\frac{\partial z}{\partial x} \tag{25}$$

thus we can reformulate Eq. (13) with vectors defined by

$$\boldsymbol{U} = \begin{bmatrix} h \\ q_x \end{bmatrix}, \quad \boldsymbol{F} = \begin{bmatrix} q_x \\ uq_x \end{bmatrix}, \quad \boldsymbol{S} = \begin{bmatrix} 0 \\ -gh\frac{\partial z}{\partial x} \end{bmatrix} \tag{26}$$

It is easy to verify that under a quiescent flow situation, the HLL flux (Eq. (18)) for the momentum equation with components defined by Eq. (26) is zero; the source term, $-gh\frac{\partial z}{\partial x}$ in Eq. (26), also vanishes. Therefore, the 1LSWE defined by Eq. (13) with components expressed in Eq. (26) is automatically pre-balanced with a simple reformulation method based on the relation described by Eq. (25). It should be noted that the solving of the 1LSWE with components defined by Eq. (26) is widely used by researchers using finite-difference or finite-element schemes (e.g., [31–33]); it is, however, seldom used with Godunov-type schemes in the framework of finite-volume methods. For briefness, the reformulation method described in this section is named balance-reformulation method hereafter. One of the main objectives of this paper is to construct a well-balanced numerical scheme for solving the 2LSWE based on the balance-reformulation idea.

2.2.2. Two-layer system balance: a first treatment

Unlike the situation in solving the 1LSWE, for which the imbalance problem is generally related to an initially quiescent flow with a flat upper-layer surface over uneven topography, various situations need to be considered when solving the 2LSWE. In Fig. 2, we summarize and list all the lake-at-rest configurations for a numerical scheme to be satisfied for solving the 2LSWE. In this and in the following two sections, we develop successively the balance treatment techniques to ensure that the stationary flows are at rest for all the configurations listed. The first case (Fig. 2(a)) is related to an initially quiescent flow with flat surface levels in both layers of same or different densities. As all the spatial derivatives

of flow variables are zero, the existing numerical schemes are capable of computing exact solutions for this situation. For the second case, as shown in Fig. 2(b), two flows of same densities over a flat bed topography are considered. The initial interface shape is irregular, but the whole layer depth H is constant over the domain. For this situation, no spurious flow should be numerically generated.

Due to the similarity between the governing equations for the upper layer (Eqs. (5) and (6)) and the 1LSWE (as described at the beginning of Section 2), the balance-reformulation method for the 1LSWE system can be directly applied for processing the upper-layer momentum equation and thus Eq. (6) becomes

$$\boldsymbol{U_2} = \begin{bmatrix} h_2 \\ q_{x2} \end{bmatrix}, \quad \boldsymbol{F_2} = \begin{bmatrix} q_{x2} \\ u_2 q_{x2} \end{bmatrix}, \quad \boldsymbol{S_2} = \begin{bmatrix} 0 \\ -gh_2 \dfrac{\partial z_2}{\partial x} \end{bmatrix} \tag{27}$$

Under the situation shown in Fig. 2(b), for the combined system (Eqs. (11) and (12)), $\chi = 1$ makes all the spatial derivatives disappear. Therefore, the combined system is numerically balanced under this configuration. As the flux gradient and the source terms in the upper-layer equations (Eqs. (5) and (27)) are also pre-balanced, the two-layer HLL approximate solver is well balanced for solving Eqs. (5) and (11) with components defined by Eqs. (27) and (12).

2.2.3. Two-layer system balance: a second treatment

In this section, we extend the numerical scheme developed in Section 2.2.2 to achieve well-balanced property under the configuration shown in Fig. 2(c). In this situation, two flows of equal density over an uneven bed topography are considered. The initial upper-layer surface is flat and the interface shape is irregular. Since the whole layer depth H varies spatially over the domain, a similar examination as presented in Section 2.2.1 for the 1LSWE system shows that the flux gradient and the bed-slope source terms in Eqs. (11) and (12) are unbalanced when the HLL approximate Riemann solver is used for numerical flux evaluations.

To tackle the imbalance problem in solving the combined system related to the situation shown in Fig. 2(c), we again adopt the balance-reformulation method here. However, this method cannot be applied directly to the combined momentum equation (Eq. (9)). In viewing that

$$gh_1h_2 + \frac{1}{2}gh_2^2 + \frac{1}{\chi}\frac{1}{2}gh_1^2 \equiv \frac{1}{2}gH^2 + \frac{1-\chi}{\chi}\frac{1}{2}gh_1^2 \tag{28}$$

and

$$-gh_2\frac{\partial z_b}{\partial x} - \frac{1}{\chi}gh_1\frac{\partial z_b}{\partial x} \equiv -gH\frac{\partial z_b}{\partial x} - \frac{1-\chi}{\chi}gh_1\frac{\partial z_b}{\partial x} \tag{29}$$

we can rewrite Eq. (9) to

$$\frac{\partial}{\partial t}\left(q_{x2} + \frac{1}{\chi}q_{x1}\right) + \frac{\partial}{\partial x}\left(u_2 q_{x2} + \frac{1}{\chi}u_1 q_{x1} + \frac{1}{2}gH^2 + \frac{1-\chi}{\chi}\frac{1}{2}gh_1^2\right) - gH\frac{\partial z_2}{\partial x} - \frac{1-\chi}{\chi}gh_1\frac{\partial z_b}{\partial x} \tag{30}$$

Application of the balance-reformulation method for treatment of the H-related terms in Eq. (30), Eq. (12) now becomes:

$$\boldsymbol{U_w} = \begin{bmatrix} h_2 + \dfrac{1}{\chi}h_1 \\[2mm] q_{x2} + \dfrac{1}{\chi}q_{x1} \end{bmatrix}, \quad \boldsymbol{S_w} = \begin{bmatrix} 0 \\[2mm] -gH\dfrac{\partial z_2}{\partial x} - \dfrac{1-\chi}{\chi}gh_1\dfrac{\partial z_b}{\partial x} \end{bmatrix}$$

$$\boldsymbol{F_w} = \begin{bmatrix} q_{x2} + \dfrac{1}{\chi}q_{x1} \\[2mm] u_2 q_{x2} + \dfrac{1}{\chi}u_1 q_{x1} + \dfrac{1-\chi}{\chi}\dfrac{1}{2}gh_1^2 \end{bmatrix} \tag{31}$$

Under the situation shown in Fig. 2(c), the terms in Eq. (31) multiplied by $(1-\chi)$ in the combined system vanish. For this reason, the momentum equation for the combined system reduced to the same form as the pre-balanced 1LSWE system expressed by Eq. (26) and is thus numerically balanced. For the upper-layer system, it is already known from Section 2.2.2 that the momentum equation is well-balanced based on Eqs. (5) and (27), and therefore, the 2LSWE defined by Eqs. (5) and (11) with components expressed by Eqs. (27) and (31), is well-balanced for the configuration shown in Fig. 2(c).

2.2.4. Two-layer system balance: further treatment

As demonstrated in Section 2.2.3, the developed numerical scheme is pre-balanced for flows with arbitrary interface shape over irregular topography if $\chi = 1$. Nevertheless, the developed numerical scheme still experiences the imbalance problem when $\chi \neq 1$ as in the situation shown in Fig. 2(d). For this configuration, the upper layer should remain steady since both its surface and bottom are flat. Also physically, the lower layer needs to be at rest since the layer-coupling

term ($\chi g h_1 \frac{\partial h_2}{\partial x}$ in Eq. (7)) does not take effect as $h_2 =$ constant (as described at the beginning of Section 2). Note that conventionally, the terminology "well-balanced" for the 2LSWE system refers to this configuration only (see, for example, [10,34]).

For the situation given in Fig. 2(d), Eq. (31) reduces to

$$\boldsymbol{U}_w = \begin{bmatrix} h_2 + \dfrac{1}{\chi} h_1 \\[2mm] q_{x2} + \dfrac{1}{\chi} q_{x1} \end{bmatrix}, \boldsymbol{F}_w = \begin{bmatrix} 0 \\[2mm] \dfrac{1-\chi}{\chi} \dfrac{1}{2} g h_1^2 \end{bmatrix}, \boldsymbol{S}_w = \begin{bmatrix} 0 \\[2mm] -\dfrac{1-\chi}{\chi} g h_1 \dfrac{\partial z_b}{\partial x} \end{bmatrix} \tag{32}$$

It is obvious that when $\frac{1-\chi}{\chi} \neq 0$ (i.e., $\chi \neq 1$), the flux gradient and the source terms in the combined momentum equation (second component of Eqs. (11) and (32)) are numerically unbalanced when the HLL approximate Riemann solver is used for numerical flux calculations. To tackle this problem, the balance-reformulation idea is adopted again. Note that

$$-\frac{\partial}{\partial x} \left(\frac{1-\chi}{\chi} \frac{1}{2} g h_1^2 \right) - \frac{1-\chi}{\chi} g h_1 \frac{\partial z_b}{\partial x} \equiv -\frac{1-\chi}{\chi} g h_1 \frac{\partial z_1}{\partial x} \tag{33}$$

then Eq. (31) can be reformulated to

$$\boldsymbol{U}_w = \begin{bmatrix} h_2 + \dfrac{1}{\chi} h_1 \\[2mm] q_{x2} + \dfrac{1}{\chi} q_{x1} \end{bmatrix}, \boldsymbol{F}_w = \begin{bmatrix} q_{x2} + \dfrac{1}{\chi} q_{x1} \\[2mm] u_2 q_{x2} + \dfrac{1}{\chi} u_1 q_{x1} \end{bmatrix}$$

$$\boldsymbol{S}_w = \begin{bmatrix} 0 \\[2mm] -gH \dfrac{\partial z_2}{\partial x} - \dfrac{1-\chi}{\chi} g h_1 \dfrac{\partial z_1}{\partial x} \end{bmatrix} \tag{34}$$

With the components defined in Eq. (34), the momentum equation for the combined system is now pre-balanced, and till now, the HLL approximate Riemann solver for solving the 2LSWE based on Eqs. (5) and (11) with components defined by Eqs. (27) and (34) are well-balanced for all the steady stationary flow configurations presented in Fig. 2 and is used in the rest of the paper.

2.2.5. Additional issue related to maintain steady stationary flow at rest

It is of great importance to note that the term "well-balanced" is commonly known to be related to the treatment of the momentum equations as discussed in Sections 2.2.1–2.2.4. Actually, even if a well-balanced numerical scheme is used for the discretization of the momentum equation, spurious flows can still be generated if the continuity equation is inappropriately discretized. For example, the standard HLL numerical flux for the upper-layer continuity equation at the interface $i − 1/2$ is calculated as (also see Eq. (17))

$$F_{2,i-1/2}^{\mathrm{HLL}_c} = \frac{S_{i-1/2}^{\mathrm{R}} F_c^{\mathrm{L}} - S_{i-1/2}^{\mathrm{L}} F_c^{\mathrm{R}}}{S_{i-1/2}^{\mathrm{R}} - S_{i-1/2}^{\mathrm{L}}} + \frac{S_{i-1/2}^{\mathrm{L}} S_{i-1/2}^{\mathrm{R}}}{S_{i-1/2}^{\mathrm{R}} - S_{i-1/2}^{\mathrm{L}}} \left(h_{2,i-1/2}^{\mathrm{R}} - h_{2,i-1/2}^{\mathrm{L}} \right) \tag{35}$$

Under a quiescent flow condition, the first part on the right-hand side (RHS) of Eq. (35) is equal to zero. The second term on the RHS of Eq. (35), however, leads to a numerical flux that either raises up or lowers down the upper-layer surface level if the Riemann states of water depth at the cell interface differ (i.e., for flows with irregular interface shape), and thus spurious flows are generated. In fact, as long as the water depth is adopted as the conserved variable for the continuity equation and without special treatment, spurious flows can be generated in solving the 1LSWE, and also in solving the upper-layer or the combined equation system related to the 2LSWE. Since $\frac{\partial z}{\partial t} \equiv \frac{\partial h}{\partial t}$ holds for the 1LSWE system over an immobile bed, recently many investigators use z instead of h as the conserved variable for the continuity equation (e.g., [21,35]). In this way, the standard HLL flux for the continuity equation expressed by Eq. (35) with a substitution of h by z, predicts accurate results under steady stationary-flow conditions. For a 2LSWE system, however, if z is used as the conserved variable in the continuity equations, source terms, e.g., for the upper layer $\frac{\partial z_1}{\partial t}$, arise in the continuity equations. As z_1 at the new time level is unavailable, explicit schemes lead to decoupled solutions for the two-layer coupled system. As was done by most of the researchers, we use h as the conserved variable in the continuity equations in this paper.

Observing that the first term on the RHS of Eq. (35) is a central difference approximation, and the second term acts as a diffusion term to stabilize the scheme [14], and in viewing that the standard HLL flux defined by Eq. (35) actually predicts promising results in unsteady flow conditions under all flow regimes [27,36,37], it is reasonable to assume that Eq. (35) may be inaccurate solely for flow with weak motions, in which case the diffusion term can be omitted to maintain the stationary flow at rest. For this reason, we modified Eq. (35) to

$$F_{2,i-1/2}^{\mathrm{HLL}_c} = \frac{S_{i-1/2}^{\mathrm{R}} F_c^{\mathrm{L}} - S_{i-1/2}^{\mathrm{L}} F_c^{\mathrm{R}}}{S_{i-1/2}^{\mathrm{R}} - S_{i-1/2}^{\mathrm{L}}} + \alpha \frac{S_{i-1/2}^{\mathrm{L}} S_{i-1/2}^{\mathrm{R}}}{S_{i-1/2}^{\mathrm{R}} - S_{i-1/2}^{\mathrm{L}}} \left(h_{2,i-1/2}^{\mathrm{R}} - h_{2,i-1/2}^{\mathrm{L}} \right) \tag{36}$$

Here, α is a parameter controlling the diffusion term of the HLL flux and in this paper is calculated by the following step function

$$\alpha = \begin{cases} 0, & \max(F_{r1,i-1}, F_{r1,i}, F_{r2,i}, F_{r2,i-1}) < F_{r\text{lmt}} \\ 1, & \text{else} \end{cases} \tag{37}$$

where F_{rk} is the internal Froude number defined as [24,25]

$$F_{rk} = \frac{|u_k|}{\sqrt{(1-\chi)gh_k}} \tag{38}$$

In case that $\chi = 1$, the following composite Froude number is used

$$F_{rk} = \frac{|q_{x1} + q_{x2}|}{\sqrt{g(h_1 + h_2)^{3/2}}} \tag{39}$$

to recover the definition of the Froude number in a one-layer shallow-water system. Though other functions (e.g., linear variation) for α can be used, we found that the step function defined by Eq. (37) performs well in all our numerical tests, as presented in Section 3, and is thus used in this paper. For the parameter $F_{r\text{lmt}}$, our numerical experiments show that it does not significantly affect the results and $F_{r\text{lmt}} = 1 \times 10^{-4}$ is chosen. For the continuity equation of the combined system, Eq. (36) also applies with a substitution of h_2 with h_w.

2.3. Source term treatment and stability criterion

Following [27,38,39], a central difference approximation is used for discretization of the source terms. For instance, for Eqs. (5) and (27) we have

$$-gh_2 \left.\frac{\partial z_2}{\partial x}\right|_i = -gh_{2,i} \frac{z_{2,i+1} - z_{2,i-1}}{2\Delta x} \tag{40}$$

a similar central difference approximation is used for the discretization of the source terms in Eqs. (11) and (34).

For time stepping, a dynamic time step is adopted according to the CFL (Courant–Friedrichs–Lewy) requirement

$$\Delta t = C_r \times \min \left(\frac{\Delta x}{\max(|S_{i-1/2}^L|, |S_{i-1/2}^R|)} \right) \tag{41}$$

where $S_{i-1/2}^L$ and $S_{i-1/2}^R$ are calculated from Eq. (20). Generally, C_r should be set to less than unity for numerical stability.

2.4. Boundary conditions

For boundary conditions, ghost cells are created outside the simulation domain. In this way, numerical fluxes at boundaries are calculated the same way as those at the interfaces between interior cells. For each layer, when the discharge is specified at a subcritical inflow boundary, the discharge at the corresponding ghost cell is set to the prescribed value, while the water depth is zeroth-order extrapolated from interior cells. When the water depth is given at a subcritical outflow boundary, the water depth at the corresponding ghost cell is set to the given value and its discharge is obtained by using a zero-gradient condition. For an open outflow boundary, both the water depth and the discharge at the ghost cells are zeroth-order extrapolated from interior cells. For a closed boundary, the water depth at the ghost cells is set to the value in the adjacent interior cells, while the discharge is given as equal but opposite to the value in its neighboring interior cells. Similar boundary condition treatment techniques are widely used in solving the 1LSWE [40,41]. Though, in principle, high-order extrapolations (e.g., [38]) or physically more accurate schemes (e.g., [42]) can be implemented, our numerical results show that the treatment described here works well and predicts favorable results.

3. Numerical tests

In this section, numerical experiments are performed to verify various properties of the developed numerical model. The test cases considered include transitional flow with hydraulic jump over a hump, smooth transcritical exchange flow over a hump, and an internal dam break wave propagating over a flat bottom.

3.1. Transitional flow with hydraulic jump over a hump

Under the rigid-lid assumption, some steady-state solutions are available for two flowing layers under particular configurations [24,25]. The rigid-lid assumption is reasonable when the difference in density between the layers is small and the

upper-layer surface is nearly flat. This test is taken from Abgrall and Karni [25]. A 6-m-long channel (-3 m $< x < 3$ m) with the following bottom topography is considered:

$$z_b(x) = \begin{cases} \frac{1}{8}\left(\cos\frac{\pi x}{2} + 1\right)^2, & |x| \le 2 \\ 0, & \text{else} \end{cases} \tag{42}$$

For boundary conditions, the discharge per unit width $q_{x1}^w = q_{x2}^w = 0.0928$ m^2/s is prescribed at the western boundary and the water depth is fixed to $h_1^e = 0.9205$ m and $h_2^e = 0.5795$ m at the eastern boundary. Here, the superscripts 'w' and 'e' denote the values at the western and eastern boundaries, respectively. Initially the flows are at rest with a flat upper-layer surface $z_2^0(x) = h_1^e + h_2^e$ and a flat interface $z_1^0(x) = h_1^e$. The superscript '0' here denotes the initial values.

The simulation is done with $\chi = 0.98$ and $g = 10$ m^2/s, using a dynamic time step with $C_r = 0.6$. The spatial step is chosen through a grid-resolution study, as stated below. Firstly, steady solutions are obtained by carrying out a series of simulations on successively finer grids. Note here that a steady solution is thought to be obtained when the globally relative change indictor, R, defined in Eq. (43), drops smaller than a critical value R_c ($R_c \to 0$). Then, when further mesh refinement causes negligible changes in the solution, the mesh is supposed to be fine enough regarding numerical accuracy.

$$R = \sqrt{\sum_{k=1}^{n_z}\sum_{i=1}^{n_x}\left(\frac{h_{k,i}^{l+1} - h_{k,i}^l}{h_{k,i}^l}\right)^2} \tag{43}$$

Here, $n_z = 2$ denotes the vertical layer numbers; n_x is the total grid number in a layer. The superscripts 'l' and '$l+1$' denote time steps. In this paper, $R_c = 1 \times 10^{-7}$ is chosen.

In Fig. 3(a), the computed interface profiles at steady states by the present model with grids from $n_x = 400$ to $n_x = 6400$ are illustrated. As seen, the solutions with $n_x = 3200$ and $n_x = 6400$ nearly coincide with each other and thus a grid of $n_x = 3200$ is chosen.

In Fig. 3(b), the computed steady solution of interface profile by the present model (with $n_x = 3200$) is compared with the rigid-lid analytic solution and the numerical result by Abgrall and Karni [25] using a relaxation approach. Note that the rigid-lid analytic solution is composed of two piecewise smooth profiles with a hydraulic jump on the right of the hump crest at $x = 0.48$ m. As seen in Fig. 3(b), both of the present model and the relaxation scheme predict reasonable results and are all in close agreement with the analytic solution. It is also noted that compared with the analytic solution, both the two numerical models predict slight discrepancy in the jump location. This discrepancy was thought to be caused due to the rigid-lid assumption in deriving the analytic solution [25]. As we check the discharges in the two layers which should be constant over the domain and over the layers, we found, as shown in Fig. 3(c), that small deviations (compared with the analytic solutions) in the predicted discharges exist near the jump location (marked out by the vertical dash-dotted line in Fig. 3(c)). The maximum relative error in discharges is about 16% (in both the two layers) between the numerical result predicted by the present model and the analytic solution. The deviation in the predicted discharges implies that the discrepancy in the predicted hydraulic jump location in this test may also be caused by the slight inaccuracy of the numerical schemes (not only due to the rigid-lid assumption, as stated in [25]). A literature review shows that similar deviation in the predicted discharge is commonly encountered for Godunov-type schemes solving the 1LSWE over an uneven topography with a hydraulic jump in the solution. For instance, in solving the one-layer steady transcritical flow with hydraulic jump over a hump, researchers reported that the predicted relative error in discharge solution is about 15%–24% when the Godunov-type schemes are employed [21,43].

The well-balanced property of the present model is tested here. All the parameters for the well-balanced test remain the same as those in the test above in this section, except that $q_{x1}^w = q_{x2}^w = 0$ is prescribed at the western boundary. In Fig. 3(d), the computed upper-layer surface and interface profiles (with $n_x = 3200$) at $t = 10$ s are presented along with the analytic solutions. It is seen that the numerical results match the analytic solutions exactly and no spurious flow is generated as expected. This clearly verifies the well-balanced property of the present model.

3.2. Smooth transcritical exchange flow over a hump

This test is taken from [25], in which rigid-lid analytic solution is provided. We use this test to check the performance of the proposed numerical scheme when the flow move in opposite directions in the layers.

The simulation domain, the bed topography, and the C_r are the same as those in the previous test (see Section 3.1). For the lower layer, $q_{x1}^w = 0.0928$ m^2/s is prescribed at the western boundary and the water depth at the eastern boundary is fixed to $h_1^e = 0.1617$ m. For the upper layer, $q_{x2}^e = -q_{x1}^w$ is applied at the eastern boundary (inlet boundary for the upper layer) and the water depth at the western boundary is set to $h_2^w = 0.4311$ m. Initially, the flows are at rest with a flat upper-layer surface $z_2^0(x) = 1.5$ m and a flat interface $z_1^0(x) = 1.0$ m. The density ratio is set to $\chi = 0.98$ and $g = 10$ m^2/s is used. Based on a grid resolution study as described in Section 3.1, a mesh with $n_x = 1600$ is chosen to ensure numerical accuracy.

In Fig. 4(a), the upper-layer surface and interface profiles at steady states computed by the present model are compared with the rigid-lid analytic solution and the numerical prediction by Abgrall and Karni [25] using a relaxation approach.
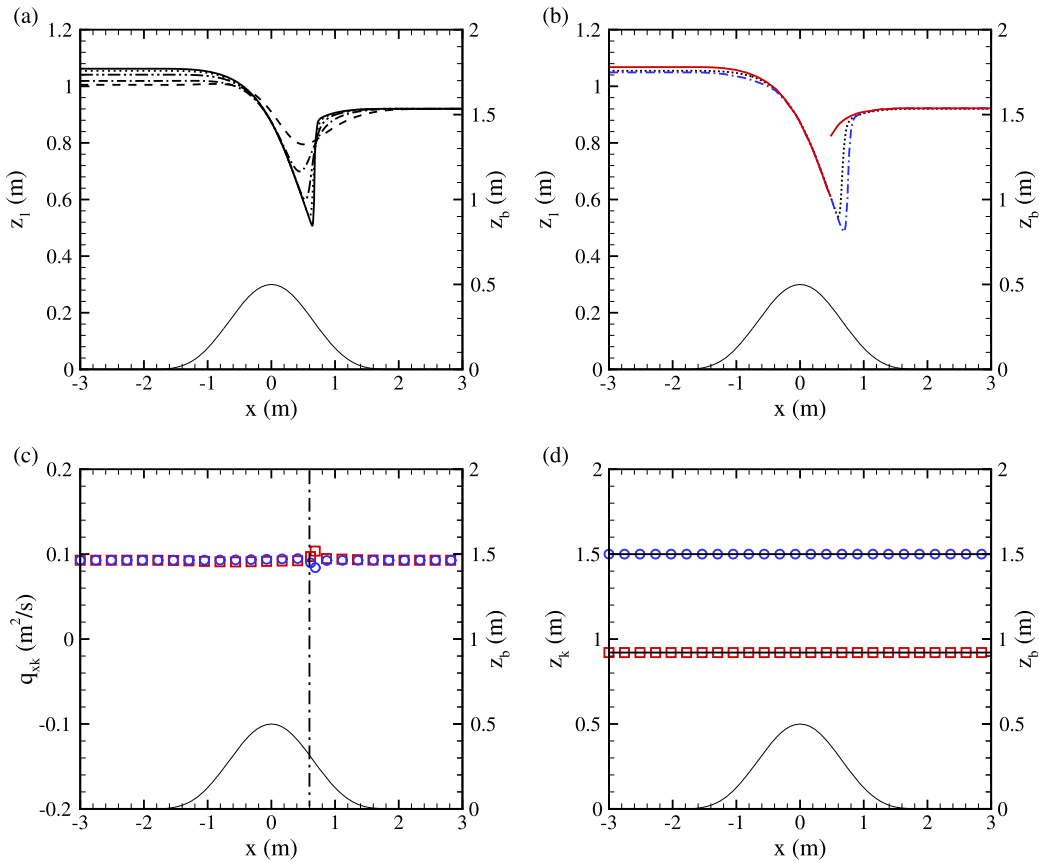
Fig. 3. (Color online.) (a) and (b) show the computed steady solutions to the interface profile obtained using the present model, with $n_x = 400$ ($- - -$), $n_x = 800$ ($- \cdot - \cdot -$), $n_x = 1600$ ($- \cdot \cdot - \cdot \cdot -$), $n_x = 3200$ ($\cdots \cdots$), and $n_x = 6400$ (——), for the transitional flow with hydraulic jump over a hump test. In (b), the numerical solution obtained using the present model with $n_x = 3200$ ($\cdots \cdots$) is compared with the analytic solution (——) and the numerical solution by Abgrall and Karni [25] ($- \cdot - \cdot -$). In (c), the computed discharges per unit width (by the present model) for the upper layer (○) and the lower layer (□) are illustrated. In (d), the computed profiles of z_2 (○) and z_1 (□) are compared with the analytic solutions (thick solid lines) for the well-balanced test. The bed topography is given at the bottom of each figure by the thin solid line and is plotted on the right y-axis.

As shown, the agreement between the predicted result by the present model and the theoretical solution is promising. Negligible difference is found between the results given by the present model and that predicted by the relaxation scheme, except that, at the upstream of the hump, our solution of the interface profile matches the theoretical solution better. In Fig. 4(b), the computed discharge in the layers at steady states by the present model along with the analytic solution are presented. As seen, the computed discharges are uniform over the domain with negative values in the upper and lower layers. The maximum difference in discharge between the numerical result computed by the present numerical model and the analytic solution is about 2%. Note that this minor discrepancy can be further lowered by using finer grids.

### 3.3. Internal dam-break wave propagation

This benchmark test is employed by many researchers to validate the numerical accuracy and robustness of their 2LSWE solvers [25,44–46]. The considered channel is of 1-m-long and the following initial conditions are used:

$$h_1^0(x) = \begin{cases} 0.5, & x < x_0, \\ 0.45, & x > x_0, \end{cases} \qquad h_2^0(x) = \begin{cases} 0.5, & x < x_0, \\ 0.55, & x > x_0 \end{cases} \qquad (44)$$

Here, x_0 denotes the initial discontinuity location in the interface profile.

Initially, uniform velocity $u_1^0(x) = u_2^0(x) = 2.5$ m/s is prescribed at each mesh point. Open boundary conditions are applied at both ends of the channel. The simulation domain is uniformly divided into 400 cells and the time step is constrained with $C_r = 0.25$. The density ration is set to $\chi = 0.98$ and $g = 10$ m^2/s is used.

Fig. 5 displays the interface profiles computed using the present model along with existing numerical solutions in the literature at various time instances. Note that the results are plotted on a relative coordinate of $x - x_0$ for convenient comparisons, as different values of x_0 are used in the literature. Previous studies show that no oscillation should be generated
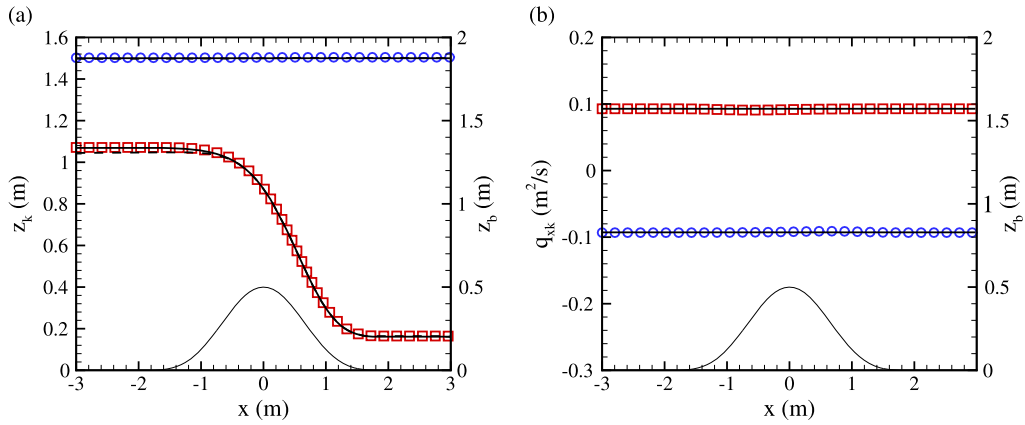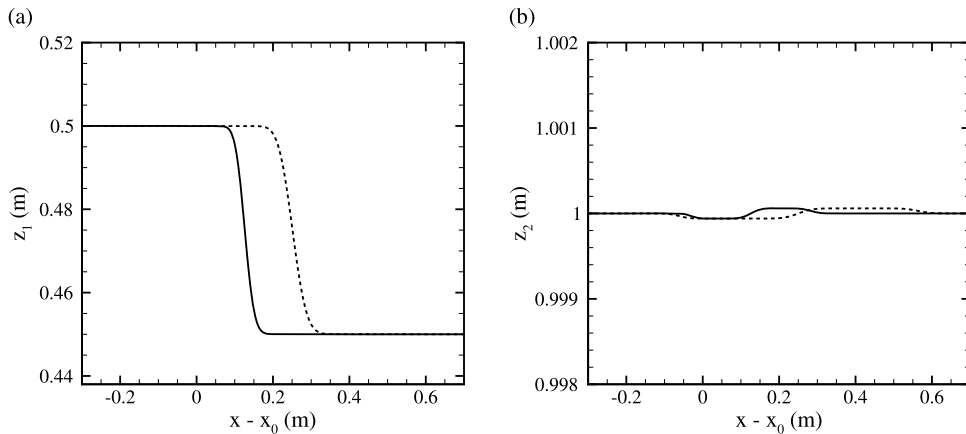
Fig. 4. (Color online.) Computed layer surface levels (a) and discharges per unit width (b) by the present model at steady states with $n_x = 1600$, for the smooth transcritical exchange flow over a hump test. The computed values for the upper- and lower-layers are marked by symbol ○ in blue and symbol □ in red, respectively. The analytic solutions are given by thick solid lines (——) in black. The bed topography is given at the bottom of each figure by the thin solid line and is plotted on the right y-axis. In (a), the numerical solution by Abgrall and Karni [25] is given by the dashed lines (– – –).
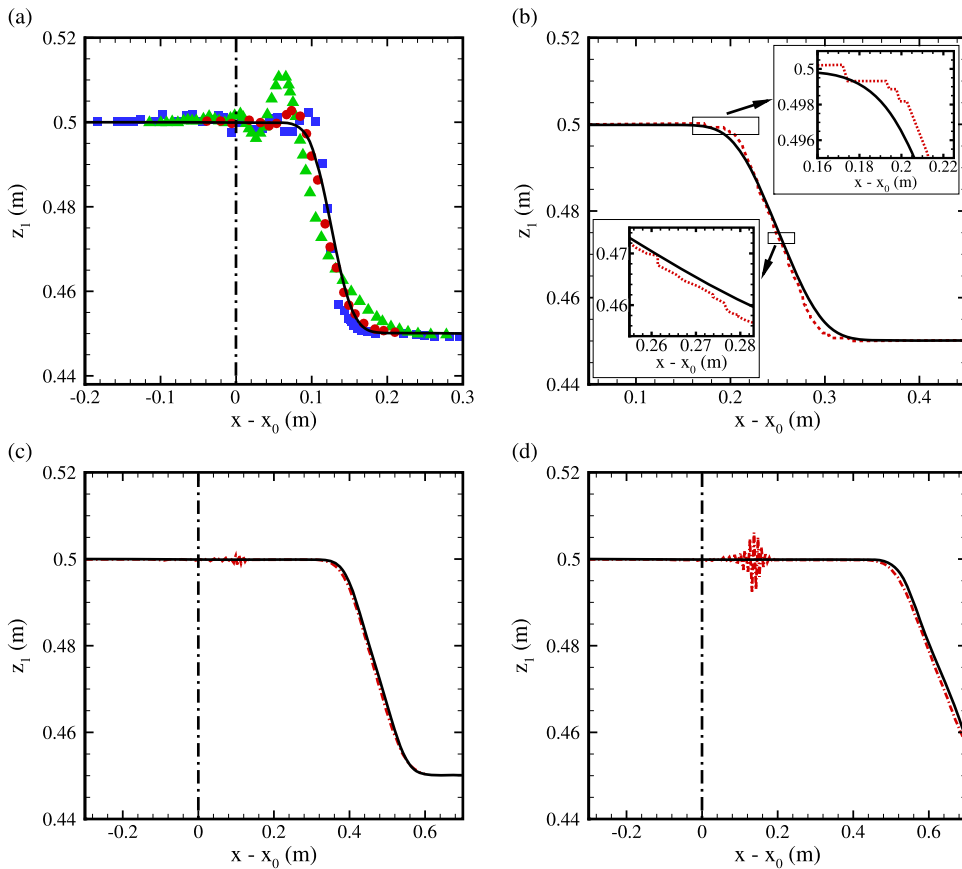
Fig. 5. (Color online.) Computed interface profiles for the internal dam-break wave propagation test with $\chi = 0.98$ by the present model (——) at $t = 0.05$ s (a), $t = 0.1$ s (b), $t = 0.1875$ s (c), and $t = 0.25$ s (d), respectively. In (a), the numerical solutions with the SCHR scheme (■) and UDCHR scheme (●) in [46], and the kinetic solver in [44] (▲), are shown. In (b), the numerical solution by the FVEG scheme in [26] is given (– – –). Zoomed views are given in (b) for clear views. In (c) and (d), the numerical solutions with the relaxation approach in [25] are shown by the dashed lines (– – –). The vertical dash-dotted line (– · – · –) represents the place where the initial discontinuity locates. Note that the region of x-axis is different among figures.

for this test [26]. However, numerical schemes without careful treatment of the non-conservative product term and the imbalance problem, can easily trigger spurious oscillations near the interface and may finally cause the code to blow up.

In Fig. 5(a), the computed interface profile by the present model is displayed at $t = 0.05$ s. Also shown are the numerical results by Bouchut and de Luna [44] using a kinetic solver, by Bouchut and Zeitlin [46] using a source-centered hydro-

Fig. 6. (Color online.) Computed interface profile (a) and upper-layer surface profile (b) by the present model, for the internal dam-break wave propagation test with $\chi = 0.995$. The solid line (——) and the dashed line (– – –) represent the numerical predictions at $t = 0.05$ s and $t = 0.1$ s, respectively.

static reconstruction scheme (abbreviated as SCHR scheme) based on Eqs. (5)–(7). The numerical result computed from a dispersive-corrected SCHR scheme [46] (abbreviated as UDCHR scheme), is also presented. As seen in Fig. 5(a), among all the numerical models, the kinetic solver exhibits the highest-amplitude oscillations. These oscillations are mainly located around the initial discontinuity location (the vertical dash-dotted line in Fig. 5(a)) and also at the front of the sharp interface around $x - x_0 = 0.1$ m. Compared with the kinetic scheme, the SCHR scheme predicts a much smoother solution, but still experiences high oscillations around the front of the sharp interface. The UDCHR scheme shows great improvement in suppressing oscillations compared with the SCHR scheme, yet it cannot eliminate the oscillations. Our present model, however, predicts no spurious oscillation at the interface between the layers.

As time evolves, e.g., from $t = 0.05$ s (Fig. 5(a)) to $t = 0.1$ s (Fig. 5(b)), the sharp front interface moves forward from $x - x_0 \approx 0.1$ m to $x - x_0 \approx 0.2$ m while the flow behind it kept almost unaffected. In Fig. 5(b), the numerical result by Dudzinski and Lukáčová-Medvid'ová [26], based on a finite-volume evolution Galerkin scheme (FVEG scheme) is also displayed. It is seen that the present model and the FVEG scheme predict nearly the same results, except that the numerical solution from the FVEG scheme is of slightly zigzag shape (see the zoomed views in Fig. 5(b)), while a smooth solution is obtained using our present model.

In Figs. 5(c) and (d), the numerical results at $t = 0.1875$ s and $t = 0.25$ s given by the present model are compared with the numerical solution by Abgrall and Karni [25] using the relaxation approach. It is seen that the results given by the two models nearly coincide with each other, except that near the area around the location $x - x_0 = 0.1$ m, the relaxation approach predicts high-frequency oscillations and it grows with time as shown in Figs. 5(c) and (d). As pointed out by Abgrall and Karni [25], the high-frequency oscillation can be suppressed by introducing sufficiently artificial viscosity to damp the instability. However, no artificial viscosity is needed to ensure numerical stability for our present model.

At the end of this section, a further numerical experiment is carried out to verify the robustness of the present model when χ approaches unity. We choose $\chi = 0.995$ and keep all other parameters as they were in the test in this section. In Fig. 6, the computed interface profile (Fig. 6(a)) and the upper-layer surface profile (Fig. 6(b)) obtained using the present model are plotted at two time instances. It is seen that the upper-layer surface and interface evolve smoothly with time, showing robustness of the numerical scheme.

4. Conclusions and discussions

In this study, a numerical model is developed for solving the two-layer shallow-water equations over an uneven topography. Based on a reformulated conservative equation system, the model is developed to numerically balance the flux gradient and the source terms under various lake-at-rest configurations. The numerical model is thoroughly tested with analytical or reference numerical solutions, under steady or unsteady flow conditions with the same or different flow directions in the layers.

The tests of steady transitional or transcritical exchange flows over a hump show that the present model is accurate and robust to capture shocks over uneven topography and to represent flow behaviors when the flows move in different directions in the layers. The internal dam break flow test further shows that the present model is stable and accurate to simulate internal wave propagations, even when the density ratio between the layers approaches unity.

As analyzed in Section 3.1, compared with the analytic solution, slight deviations in discharge and hydraulic jump location are predicted around the hydraulic jump region over an uneven topography. Actually this is an inherent characteristic of most finite-volume Godunov-type schemes and a progress in devising schemes for obtaining exactly steady moving flow solutions would help gain more accurate solutions for layered flows over an uneven topography. Further work also needs to be done to better approximate the numerical mass flux when the water depth is chosen as the conserved variable. The

modified HLL flux proposed in this paper is mainly motivated by our wish to obtain exact lake-at-rest solutions; though it works well in all the tests considered in this paper, further validation or improvement of the proposed scheme is needed. Wetting–drying is another important issue to be addressed for solving the two-layer shallow-water system, and it will be implemented in the future.

Acknowledgements

References

[1] S.-C. Chen, S.-H. Peng, H. Capart, Two-layer shallow water computation of mud flow intrusions into quiescent water, J. Hydraul. Res. 45 (2007) 13–25.
[2] Y. Hu, X. Guo, X. Lu, Y. Liu, R.A. Dalrymple, L. Shen, Idealized numerical simulation of breaking water wave propagating over a viscous mud layer, Phys. Fluids 24 (2012) 112104.
[3] S.B. Dalziel, Two-layer hydraulics: a functional approach, J. Fluid Mech. 223 (2006) 135–163.
[4] T. Gerkema, J. Zimmerman, An Introduction to Internal Wave, Lecture Notes, Royal NIOZ, Texel, 2008.
[5] W.-K. Lee, A.G.L. Borthwick, P.H. Taylor, Wind-induced chaotic mixing in a two-layer density-stratified shallow flow, J. Hydraul. Res. 52 (2014) 219–227.
[6] E.F. Toro, Shock-Capturing Methods for Free-Surface Shallow Flows, Wiley, 2001.
[7] E.F. Toro, P. Garcia-Navarro, Godunov-type methods for free-surface shallow flows: a review, J. Hydraul. Res. 45 (2007) 736–751.
[8] S.C. Medeiros, S.C. Hagen, Review of wetting and drying algorithms for numerical tidal flow models, Int. J. Numer. Methods Fluids 71 (2013) 473–487.
[9] A. Kurganov, G. Petrova, Central-upwind schemes for two-layer shallow water equations, SIAM J. Sci. Comput. 31 (2009) 1742–1773.
[10] M. Dumbser, M. Castro, C. Parés, E.F. Toro, ADER schemes on unstructured meshes for nonconservative hyperbolic systems: applications to geophysical flows, Comput. Fluids 38 (2009) 1731–1748.
[11] M.J. Castro-Díaz, E.D. Fernández-Nieto, J.M. González-Vida, C. Parés-Madroñal, Numerical treatment of the loss of hyperbolicity of the two-layer shallow-water system, J. Sci. Comput. 48 (2011) 16–40.
[12] G. Dal Maso, P. LeFloch, F. Murat, Definition and weak stability of non-conservative products, J. Math. Pures Appl. 74 (1995) 483–548.
[13] R. Abgrall, S. Karni, A comment on the computation of non-conservative products, J. Comput. Phys. 229 (2010) 2759–2763.
[14] B. Spinewine, V. Guinot, S. Soares-Frazão, Y. Zech, Solution properties and approximate Riemann solvers for two-layer shallow flow models, Comput. Fluids 44 (2011) 202–220.
[15] A. Bermudez, M. Vazquez, Upwind methods for hyperbolic conservation laws with source terms, Comput. Fluids 23 (1994) 1049–1071.
[16] S. Bryson, Y. Epshteyn, A. Kurganov, G. Petrova, Well-balanced positivity preserving central-upwind scheme on triangular grids for the Saint-Venant system, Modél. Math. Anal. Numér. 45 (2011) 423–446.
[17] M. Kazolea, A.I. Delis, A well-balanced shock-capturing hybrid finite volume–finite difference numerical scheme for extended 1D Boussinesq models, Appl. Numer. Math. 67 (2013) 167–186.
[18] J.G. Zhou, D.M. Causon, C.G. Mingham, D.M. Ingram, The surface gradient method for the treatment of source terms in the shallow-water equations, J. Comput. Phys. 168 (2001) 1–25.
[19] E. Audusse, F. Bouchut, M.-O. Bristeau, R. Klein, B. Perthame, A fast and stable well-balanced scheme with hydrostatic reconstruction for shallow water flows, SIAM J. Sci. Comput. 25 (2004) 2050–2065.
[20] B. Rogers, M. Fujihara, A.G.L. Borthwick, Adaptive Q-tree Godunov-type scheme for shallow water equations, Int. J. Numer. Methods Fluids 35 (2001) 247–280.
[21] Q. Liang, A.G.L. Borthwick, Adaptive quadtree simulation of shallow flows with wet–dry fronts over complex topography, Comput. Fluids 38 (2009) 221–234.
[22] W.-K. Lee, A.G.L. Borthwick, P.H. Taylor, On mathematical balancing of a two-layer shallow flow model, in: Proceedings of the First IAHR European IAHR Congress, Edinburgh, UK, 2010.
[23] W.-K. Lee, A.G. Borthwick, P.H. Taylor, A fast adaptive quadtree scheme for a two-layer shallow water model, J. Comput. Phys. 230 (2011) 4848–4870.
[24] L. Arm, The hydraulics of two flowing layers with different densities, J. Fluid Mech. 163 (1986) 27–58.
[25] R. Abgrall, S. Karni, Two-layer shallow water system: a relaxation approach, SIAM J. Sci. Comput. 31 (2009) 1603–1627.
[26] M. Dudzinski, M. Lukáčová-Medvid'ová, Well-balanced bicharacteristic-based scheme for multilayer shallow water flows including wet/dry fronts, J. Comput. Phys. 235 (2013) 82–113.
[27] Z. Cao, G. Pender, S. Wallis, P. Carling, Computational dam-break hydraulics over erodible sediment bed, J. Hydraul. Eng. 130 (2004) 689–703.
[28] A. Harten, P.D. Lax, B. van Leer, On upstream differencing and Godunov-type schemes for hyperbolic conservation laws, SIAM Rev. 25 (1983) 35–61.
[29] E.F. Toro, M. Spruce, W. Speares, Restoration of the contact surface in the HLL-Riemann solver, Shock Waves 4 (1994) 25–34.
[30] S. Davis, Simplified second-order Godunov-type methods, SIAM J. Sci. Stat. Comput. 9 (1988) 455–473.
[31] X. Lu, B. Dong, B. Mao, X. Zhang, Unstructured mixed grid and SIMPLE algorithm based model for 2D-SWE, Proc. Eng. 28 (2012) 117–121.
[32] V. Rostand, D.Y.L. Roux, G. Carey, Kernel analysis of the discretized finite difference and finite element shallow-water models, SIAM J. Sci. Comput. 31 (2008) 531–556.
[33] R. Comblen, S. Legrand, E. Deleersnijder, V. Legat, A finite element method for solving the shallow water equations on the sphere, Ocean Model. 28 (2009) 12–23.
[34] K.T. Mandli, A numerical method for the two layer shallow water equations with dry states, Ocean Model. 72 (2013) 80–91.
[35] M.E. Hubbard, N. Dodd, A 2D numerical model of wave run-up and overtopping, Coast. Eng. 47 (2002) 1–26.
[36] W. Wu, R. Marsooli, A depth-averaged 2D shallow water model for breaking and non-breaking long waves affected by rigid vegetation, J. Hydraul. Res. 50 (2012) 558–575.
[37] G. Kesserwani, Topography discretization techniques for Godunov-type shallow water numerical models: a comparative study, J. Hydraul. Res. 51 (2013) 351–367.
[38] X. Ying, S.S.Y. Wang, Improved implementation of the HLL approximate Riemann solver for one-dimensional open channel flows, J. Hydraul. Res. 46 (2008) 21–34.
[39] S. Erpicum, B. Dewals, P. Archambeau, M. Pirotton, Dam break flow computation based on an efficient flux vector splitting, J. Comput. Appl. Math. 234 (2010) 2143–2151.
[40] T.G. Jensen, Open boundary conditions in stratified ocean models, J. Mar. Syst. 16 (1998) 297–322.

[41] B.F. Sanders, High-resolution and non-oscillatory solution of the St. Venant equations in non-rectangular and non-prismatic channels, J. Hydraul. Res. 39 (2001) 321–330.
[42] J. Nycander, A.M. Hogg, L.M. Frankcombe, Open boundary conditions for nonlinear channel flow, Ocean Model. 24 (2008) 108–121.
[43] A. Valiani, L. Begnudelli, Divergence form for bed slope source term in shallow water equations, J. Hydraul. Eng. 132 (2006) 652–665.
[44] F. Bouchut, T.M. de Luna, An entropy satisfying scheme for two-layer shallow water equations with uncoupled treatment, Modél. Math. Anal. Numér. 42 (2008) 683–698.
[45] M. Castro, J. Macías, C. Parés, A Q-scheme for a class of systems of coupled conservation laws with source term. Application to a two-layer 1-D shallow water system, Modél. Math. Anal. Numér. 35 (2001) 107–127.
[46] F. Bouchut, V. Zeitlin, A robust well-balanced scheme for multi-layer shallow water equations, Discrete Contin. Dyn. Syst., Ser. B 13 (2010) 739–758.